Acoustic noise of electromagnetic origin in a fractional-slot induction machine

Jean Le Besnerais*, Vincent Lanfranchi†, Michel Hecquet*, Pascal Brochet* and Guy Friedrich†
* *L2EP - Ecole Centrale de Lille, Villeneuve d'Ascq, France (jean.le_besnerais@centraliens.net)*
† *LEC - UTC, Compiègne, France (vincent.lanfranchi@utc.fr)*

Abstract

Purpose - The main purpose of this paper is to apply a fast analytical model of the acoustic behaviour of pulse-width modulation (PWM) controlled induction machines (Besnerais, Fasquelle, Hecquet, Lanfranchi & Brochet 2006) to a fractional-slot winding machine. A second goal is to analytically clarify the interaction between space harmonics and time harmonics in audible electromagnetic noise spectrum.

Methodology/approach - A multilayer single-phase equivalent circuit calculates the stator and rotor currents. Air-gap radial flux density, which is supposed to be the only source of acoustic noise, is then computed with winding functions formalism. Mechanical and acoustic models are based on a 2D ring stator model. A method to analytically derive the orders and frequencies of most important vibration lines is detailed. The results are totally independent of the supply strategy and winding type of the machine. Some variable-speed simulations and tests are run on a 700 W fractional-slot induction machine in sinusoidal case as a first validation of theoretical results.

Findings - The influence of both winding space harmonics and PWM time harmonics on noise spectrum is exposed. Most dangerous orders and frequencies expressions are demonstrated in sinusoidal and PWM cases. For traditional integral windings, it is shown that vibration orders are necessarily even. When stator slot number is not even, which is the case for fractional windings, some odd order deflection appear: the radial electromagnetic power can therefore dissipate as vibrations through all stator deformation modes, leading to a potentially lower noise level at resonance.

Research limitations - The analytical work of this paper does not consider saturation and eccentricity harmonics which can play a significant role in noise radiation.

Practical implications - The analytical model and theoretical results presented in this paper help designing low-noise induction machines, and diagnosing noise or vibration problems.

Originality/value - This paper details a fully analytical acoustic and electromagnetic model of a PWM fed induction machine, and demonstrate the theoretical expression of main noise spectrum lines combining both time and space harmonics.

Keywords - Induction machine, Magnetic noise, Vibrations, Fractional-slot winding.

Paper type - Research paper.

NOMENCLATURE

Electrical notations

f_s	Fundamental stator supply frequency
f^r_{mn}	Rotor current n-th time and m-th space harmonic
f^s_n	Stator current n-th time harmonic
f_{mm}	Magnetomotive force
f_R	Mechanical rotation frequency ($f_R = (1-s)f_s/p$)
F_r, F_s	Rotor and stator mmf waves
g	Air-gap width
h_r,h_s	Integers involved in rotor and stator mmf space harmonics expression
i^r_b	b-th rotor bar current
i^s_q	q-th stator phase current
k_r, k_s	Integers involved in rotor and stator slotting terms in permeance Fourier series
l_{sd}	Stator tooth width
l_{se}	Stator slot opening width
l_{rd}	Rotor tooth width
l_{re}	Rotor slot opening width
L_n	Force line number n
m	m-th space harmonic induced by stator winding in rotor bars currents (fundamental $m = p$)
n	n-th time harmonic generated by PWM supply (fundamental $n = 1$)

p	Number of pole pairs
P_r, P_s	Rotor and stator slotting permeance waves
q_s	Number of stator phases
s_{mn}	Harmonic slip (fundamental $s_{p1} = s$)
U_n	n-th time harmonic of PWM phase voltage
Z_r	Number of rotor slots
Z_s	Number of stator slots
α_r	Rotor angular position in stator steady frame
α_r^k	k-th rotor slot angular position
α_s	Angular position in stator steady frame
α_s^k	k-th stator slot angular position
β_r	Rotor slot half angular width
ϵ_r, ϵ_s	± 1 factor representing rotor or stator mmf wave direction
η_{ij}	± 1 factor resulting from the interaction of fields i and j
Λ	Permeance per unit area
ν_s,ν_r	Stator and rotor mmf space harmonics
ω_n	n-th time harmonic pulsation coming from PWM
θ_r^k	Angular position of k-th rotor tooth
Ξ_m	Winding factor of m-th space harmonic

Mechanical and acoustic notations

D_c	Stator core outer radius (without frame)
f	Exciting force frequency
f_m	m-th mode natural frequency
h_c	Height of stator yoke
L_r	Rotor stack length
L_s	Stator stack length
m	m-th circumferential spatial mode
R_a	Stator bore radius
R_c	Stator mean radius (computed without teeth)
R_e	Stator core outer radius
R_i	Stator slots bottom radius
$Y_{m\omega}^d$	Dynamic deflection of order m at pulsation ω
$Y_{m\omega}^s$	Static deflection of order m at pulsation ω
ξ_m	m-th mode damping coefficient

I. Introduction

As acoustic norms become stricter in power electrical transport systems, understanding and predicting noise of electromagnetic origin at variable speed is crucial. In fact, Pulse-Width Modulation (PWM) strategies add many harmonics to the air-gap Maxwell forces spectrum, leading to possibly harmful noise and vibrations. Stator windings induce in rotor currents additional time harmonics which can also significantly enrich the electromagnetic forces spectrum, especially when running at high slip. Audible electromagnetic noise spectrum therefore results from a complex combination of both PWM time harmonics and winding space harmonics. Predicting this so-called ”magnetic noise” level requires to precisely model both the mechanical structure of the machine and its electromagnetic excitation.

This paper presents a simulation tool of the PWM-fed induction machine, Diva (Besnerais et al. 2006, Ait-Hammouda 2005), which is able to consider the whole space and time harmonics involved in magnetic noise generation without a prohibitive computation time. Some validations by FEM or tests are presented at different levels of modelization. The analytical derivation of main radial force lines spatial modes and frequencies is exposed, including the influence of stator winding and rotor bars space harmonics. Finally, some variable-speed simulations are analyzed on the ground of these theoretical results. The acoustic role of odd spatial modes will be also discussed.

The motor studied in this paper is a 700 W three-phase squirrel-cage induction machine with p=2 pole pairs, Z_r=21 rotor bars and Z_s=27 stator slots. Its double-layer winding is a fractional-slot winding as its number of slot per pole and per phase is not an integer.

II. Electromagnetic model

A. Currents computation

Supply phase voltage can be either given by experimental data or computed analytically. Then, stator and rotor phase currents are computed using an extension of the fundamental single-phase equivalent circuit, including all space and time harmonics

(Hubert 2000). As illustrated in Fig. 1, at each time harmonic U^n of frequency f_n^s coming from the PWM supply phase voltage corresponds an equivalent circuit including the influence of m [1] stator winding space harmonics.

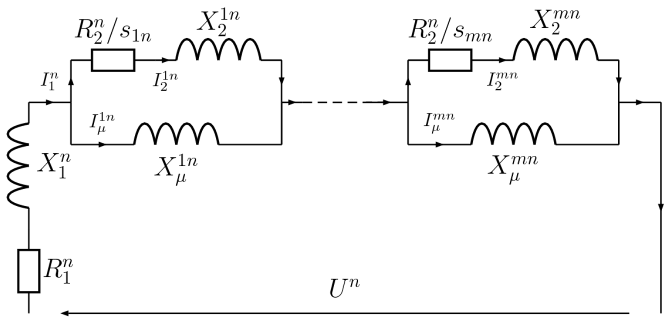

Fig. 1. Multi-layer single phase equivalent circuit

The equations of this equivalent circuit consist in n global mesh equations

$$\begin{aligned} U^n &= (R_1^n + jX_1^n)I_1^n + \textstyle\sum_m jX_\mu^{mn} I_\mu^{mn} \\ &\doteq Z_1^n I_1^n + \textstyle\sum_m Z_\mu^{mn} I_\mu^{mn} \end{aligned} \tag{1}$$

$m \times n$ node equations

$$I_1^n = I_\mu^{mn} + I_2^{mn} \tag{2}$$

and $m \times n$ local mesh equations

$$\begin{aligned} 0 &= jX_\mu^{mn} I_\mu^{mn} - (jX_2^{mn} + R_2^n/s_{mn}) I_2^{mn} \\ &\doteq Z_\mu^{mn} I_\mu^{mn} - Z_2^{mn} I_2^{mn} \end{aligned} \tag{3}$$

R_1^n and R_2^n respectively stand for the stator and rotor equivalent resistances which depend on time harmonics because of skin effect. The detailed expression of this effect can be found for instance in (Matsuse, Hayashida, Kubota & Yoshida 1994).

$X_1^n = \omega_n L_1 = 2\pi f_s^n L_1$ is the stator total phase reactance, L_1 being the corresponding inductance. $X_2^{mn} = \omega_n L_2^m$ is the rotor total reactance, L_2^m being the rotor inductance refered to the primary. It depends on space harmonics m because it is proportional to the transformation factor which is a function of the winding distribution factors Ξ_m. The expression of these distribution factors can be found for instance in (Salminen 2004) for both integral and fractional-slot windings.

$X_\mu^{mn} = \omega_n L_\mu^m$ is the magnetizing reactance in which we can eventually include a parallel iron losses equivalent resistance. L_μ^m is a generalization of the fundamental magnetizing inductance L_μ^p (Hubert 2000)

$$L_\mu^m = L_\mu^p \left(\frac{p}{m} \frac{\Xi_m}{\Xi_p} \right)^2 \tag{4}$$

where Ξ_m is the winding factor of the m-th space harmonic generated by the stator winding.

I_2^{mn} and I_1^n are the harmonic rotor and stator currents, I_μ^{mn} is the harmonic magnetizing current. s_{mn} is the harmonic slip

$$s_{mn} = 1 \pm \frac{m\omega_1}{p\omega_n}(1-s) \tag{5}$$

where s is the fundamental slip and the ± 1 factor takes into account the propagation direction of harmonic fields induced by stator currents.

For a given time harmonic n, $2m+1$ equations can be grouped in the following matrix form

$$\mathbf{Z^n}.\mathbf{I^n} = \mathbf{U^n} \tag{6}$$

with

$$\mathbf{Z^n} = \begin{pmatrix} Z_1^n & \mathbf{Z}_\mu^n & \mathbf{0} \\ \mathbf{1} & -\mathbb{I} & -\mathbb{I} \\ \mathbf{0} & \mathbf{D}_\mu^n & -\mathbf{D}_2^n \end{pmatrix} \quad \mathbf{I^n} = \begin{pmatrix} I_1^n \\ \mathbf{I}_\mu^n \\ \mathbf{I}_2^n \end{pmatrix} \quad \mathbf{U^n} = \begin{pmatrix} U^n \\ \mathbf{0} \\ \mathbf{0} \end{pmatrix}$$

[1]We define the space harmonics as the "spatial frequencies" coming from the Fourier Transform of a function of the mechanical angle, not of the electrical angle. With such a definition, the space fundamental is the number of pole pairs p and not 1.

where $\mathbf{1}$ is the unitary vector, $\mathbb{I}$ the identity matrix, $\mathbf{0}$ the null matrix, $\mathbf{Z}_\mu^n$ the Z_μ^{mn} line vector, $\mathbf{D}_\mu^n$ the Z_μ^{mn} diagonal matrix and $\mathbf{D}_2^n$ the Z_2^{mn} diagonal matrix, $\mathbf{I}_2^n$ the I_2^{mn} column vector and $\mathbf{I}_\mu^n$ the I_μ^{mn} column vector. System (6) is solved for each non-zero time harmonic U^n.

B. *Air-gap radial flux density computation*

Radial air-gap flux density B_g is expressed as

$$B_g(t, \alpha_s) = \Lambda(t, \alpha_s) f_{mm}(t, \alpha_s) \tag{7}$$

where α_s is the angular position in the stator steady frame, $\Lambda = \mu_0/g_e$ is the air-gap permeance per unit area, g_e being the effective air-gap width (detailed in section V-A) and μ_0 the air-gap magnetic permeability, and f_{mm} is the total magnetomotive force (mmf). Applying the Ampere's law to an appropriate path, one can show (Bossio, Angelo, Solsona, Garcia & Valla 2004) that

$$f_{mm}(t, \alpha_s) = \underbrace{\sum_{q=1}^{q_s} i_q^s(t) N_q^s(\alpha_s)}_{f_{mm}^s} + \underbrace{\sum_{b=1}^{Z_r} i_b^r(t) N_b^r(t, \alpha_s)}_{f_{mm}^r} \tag{8}$$

where N_q^s is the 2-D turns function (TF) or winding distribution function associated to the stator q-th phase with current i_q^s, and N_b^r is the turns function associated to the rotor b-th bar with current i_b^r. Note that contrary to stator TFs, rotor TFs are time-dependent.

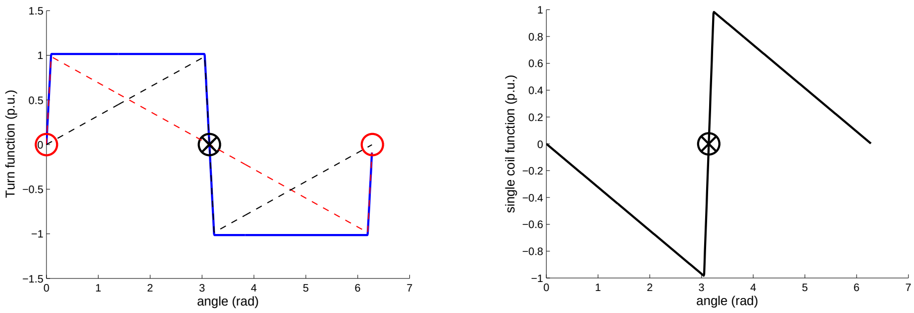

Fig. 2. Normalized full-pitch winding distribution function N_q^s (left) and the equivalent normalized coil distribution function (right).

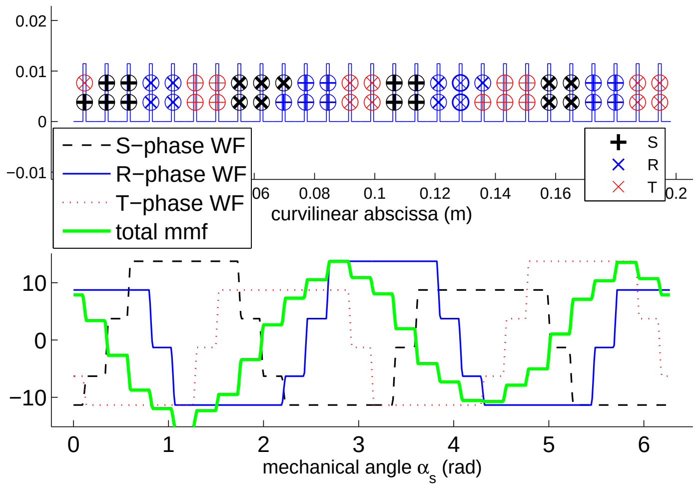

Fig. 3. Winding functions and total stator magnetomotive force at a given time

Normalized phase TF of a full-pitch winding is represented in FIG. 2, including a linear rise in slots. It can be computed summing some equivalent coil turns functions weighted with current sign. That decomposition and the winding function formalism have been chosen to be implemented in DIVA because they allow modelling any type of winding, especially fractional-slot ones. Phase TFs and the resulting stator mmf of the double-layer fractional-slot test motor are displayed in FIG. 3.

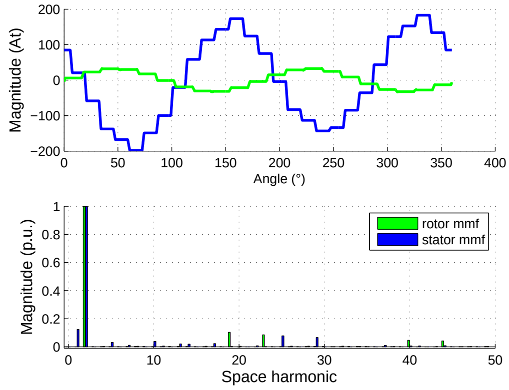

Fig. 4. Rotor and stator mmf as a function of mechanical angle and their normalized space harmonic content at a given time.

In order to compute the squirrel-cage rotor mmf, rotor cage can be viewed as an equivalent Z_r-phase circuit with Z_r loop currents (Henao, Razik & Capolino 2005, Joksimovic, Djurovic & Penman 2001). In that case, turns functions can still be used but with an equivalent number of turns of 1.

Stator and rotor mmf of test motor as well as their space harmonic content are shown in FIG. 4 in sinusoidal on-load case, with a 3.05% slip. We can see that rotor mmf wave tends to counterbalance stator mmf wave as predicted by Lenz law. Besides fundamental at $\nu_r = p$, rotor mmf contains main space harmonics $\nu_r = 19$ and 23 corresponding to $\nu_r = Z_r \pm p$. The same analysis can be carried with stator mmf which contains main space harmonics $\nu_s = Z_s \pm p$. Spectral contents of stator and rotor mmfs are detailed later in section V-B.

C. Validation

Radial air-gap flux density has been compared to finite element method (FEM) simulations for different shorted-pitch machines, supply frequencies and voltages. Motor torque and phase current were also validated with FEM and experiments in on-load case (Besnerais et al. 2006).

III. MECHANICAL MODEL

A. Exciting force computation

Neglecting Maxwell tensor's tangential component and magnetostrictive effect, the exciting pressure P_M responsible for magnetic noise can be approximated by

$$P_M = \frac{B_g^2}{2\mu_0} \tag{9}$$

B. Stator deflections computation

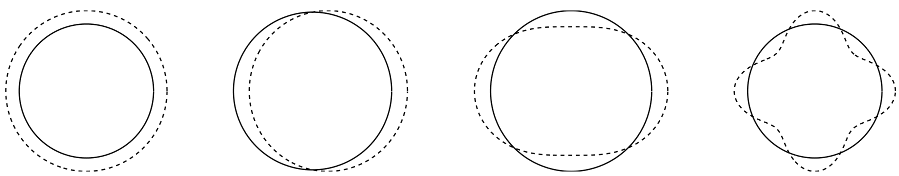

Fig. 5. Shape of circumferential spatial modes $m = 0$, $m = 1$, $m = 2$ and $m = 4$.

The mechanical model assumes that the stator is a 2D ring with free-free boundary conditions. Therefore, only in-plane circumferential spatial modes m are considered (see FIG. 5). However, we will see that the third dimension is taken into account through rotor bending motion. Static deflections $Y_{m\omega}^s$ are first computed in function of $P_{m\omega}$, the complex components P_M 2-D discrete Fourier transform. Their amplitudes are found using theory for a simply supported beam carrying a sinusoidally distributed load (Jordan 1950). For $m = 0$,

$$Y^s_{0\omega} = P_{0w}\frac{R_c R_a}{E_c h_c} \tag{10}$$

where h_c is the thickness of the stator back, R_c is the mean stator radius, R_a is the stator bore radius and E_c is the stator Young modulus. $Y^s_{1\omega}$ is generated by the force per unit area $P_{1\omega}$ which excites the rotor (cf. FIG. 5), it corresponds to a bending motion in longitudinal direction. Such a deflection can be approximated considering the rotor as a simply supported beam loaded with pressure $P_{1\omega}$:

$$Y^s_{1\omega} = P_{1\omega}\frac{4R_a l_{sh}^3 L_r}{3E_{sh} D_{sh}^4} \tag{11}$$

where L_r stands for rotor length, E_{sh} for rotor shaft Young modulus, D_{sh} for its diameter and l_{sh} for the distance between bearings. Finally, for orders $m \geq 2$,

$$Y^s_{m\omega} = P_{m\omega}\frac{12R_a R_c^3}{E_c h_c^3 (m^2-1)^2} \tag{12}$$

Then, dynamic deflections $Y^d_{m\omega}$ are computed as

$$Y^d_{m\omega} = Y^s_{m\omega}[\left(1 - f^2/f_m^2\right)^2 + 4\xi_m^2 f^2/f_m^2]^{-1/2} \tag{13}$$

where ξ_m is the modal damping coefficient, and f_m is the m-th mode natural frequency. ξ_m can be computed using the experimental law established by (Yang 1981)

$$2\pi\xi_m = 2.76 \times 10^{-5} f_m + 0.062 \tag{14}$$

In (13), the second order magnification factor comes from the fact that any excited system motion is ruled by a second order differential equation. The damping coefficient quantifies how much kinetic energy decays through Coulomb and viscous frictions, which mainly occur in lamination, windings and insulation (Verma & Balan 1998). This filter also models the resonance phenomenon: a dynamic deflection of mode m is the highest when the exciting frequency f is the closest from the natural frequency f_m. At resonance, dynamic deflections are given by

$$Y^d_{m\omega} = \frac{Y^s_{m\omega}}{2\xi_m} \tag{15}$$

Thus, the more there are damping materials, the lower vibrations occur. From (10) and (12), it can be also deduced that

$$\frac{Y^d_{m\omega}}{Y^d_{0\omega}} \propto \frac{P_{m\omega}}{P_{0\omega}}\frac{R_c^2}{h_c^2} \tag{16}$$

Therefore, R_c/h_c ratio sizes the ability of the stator to radiate vibrations : the higher R_c is and the lower h_c is, the larger and the thinner the stator is, and the more it plays the role of sound box. Nevertheless, decreasing R_c at constant h_c does not necessarily decrease noise because stator radiation efficiency increases with $L_f/R_f \approx L_s/R_c$ ratio (Gieras 2005).

C. Natural frequencies computation

1) Expression: Analytical prediction of f_m natural frequencies is a difficult task. In our case, winding and teeth effects are taken into account by modifying stator mass density ρ_c, defining

$$\rho_c' = k_s\frac{M_t + M_c}{\pi L_s(R_c^2 - R_a^2)} \tag{17}$$

where k_s is the stator stacking factor, M_t the teeth mass, M_c the stator yoke mass, L_s the stator length, R_e the stator core outer radius and R_i the stator slots bottom radius. Windings and insulation mass was therefore neglected, which might be only applicable to small machines.

Zero-th mode order natural frequency is

$$f_0 = \frac{1}{2\pi R_c}\sqrt{\frac{E_c}{\rho_c'}} \tag{18}$$

Mode number 1 natural frequency can be approximated treating the rotor and its shaft as a simply supported beam with a ring (Maliti 2000). Shaft stiffness is

$$K_{sh} = \frac{3\pi E_{sh} D_{sh}}{4l_{sh}^3} \tag{19}$$

Modal mass M_r equals rotor ring mass plus half shaft mass. We obtain:

$$f_1 = \frac{1}{2\pi}\sqrt{\frac{K_{sh}}{M_r}} \tag{20}$$

This is a very simple model as it does not consider rotor lamination stiffness and assumes that bearings are rigid. m-th mode natural frequency ($m \geq 2$) is

$$f_m = f_0 \Gamma \frac{m(m^2-1)}{\sqrt{m^2+1}} \qquad \Gamma = \frac{h_c}{2\sqrt{3}R_c} \tag{21}$$

Finally, in order to take into account the three-dimensional effects, these frequencies f_m are mutiplied by additional factors K_m (Cremer, Heckl & Ungar 1988): $K_2 = 1.14$, $K_3 = 1.04$ and $K_4 = 1.02$.

Notice that

$$f_m \approx \frac{1}{R_c}\frac{h_c}{R_c} = \frac{h_c}{R_c^2} \tag{22}$$

Thus, increasing h_c/R_c ratio in order to limit vibrations will also increase stator natural frequencies.

2) Validation: Induction machine natural frequencies have been calculated by 2-D FEM, and measured by shock and sinus methods (Hubert & Friedrich 2002). Comparison with the analytical method are presented in Table I. There is a good agreement between analytical results and experiments, because test motor geometry is rather simple (thin circular frame). The analytical computation of mode 1 natural frequency is the most inaccurate, as bearings stiffness is not considered and the measurement of bearings distance was not very precise.

TABLE I

RESULTS OF DIFFERENT METHODS FOR STATOR NATURAL FREQUENCIES COMPUTATION (HZ). OR: OUT OF RANGE, ND: NON DEFINITE.

m	Analytical	2-D FEM	Shock Method	Sinus Method
0	14859	14656	OR	OR
1	1100	ND	1200	1273
2	2478	2364	2400	2423
3	6396	6473	6100	6210
4	12028	11898	11700	OR

D. Vibration velocity and acceleration computation

1) Expression: Vibration velocity waves are given by $v_{m\omega} = Y^d_{m\omega} 2\pi f$, and acceleration waves are $a_{m\omega} = v_{m\omega} 2\pi f$.

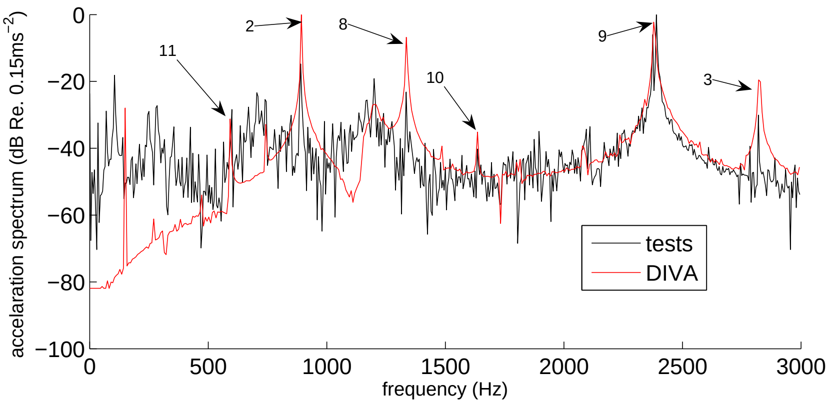

Fig. 6. Comparison between experimental and simulated acceleration spectra at $f_s = 75$ Hz and $s = 5.6$ % in sinusoidal case.

2) Validation: FIG. 6 compares simulated and experimental stator frame acceleration spectra at supply frequency $f_s = 75$ Hz, and slip $s = 5.6$ %, in sinusoidal case. High differences appear under 500 Hz, which mainly come from mechanical vibrations that are not included in the model. We can see that DIVA simulation tool correctly predicts main vibration lines. Their expression can be found with analytical results of section V: for instance, the 2800 Hz line (number 3) is of order $1 = 3Z_s - 4Z_r + 2p$ and frequency $f_s(4(1-s)\frac{Z_r}{p} - 2)$, and the 900 Hz line (number 2) is of order $2 = Z_s - Z_r - 2p$ and frequency $f_s((1-s)\frac{Z_r}{p} + 2)$.

IV. ACOUSTIC MODEL

Sound power radiated by vibrations of mode m and frequency f is

$$W_m(f) = \frac{1}{2}\rho_0 c_0 S_c \sigma_m(f) < \overline{v_{m\omega}^2} > \quad (23)$$

where S_c is the stator outer surface, ρ_0 the air density, c_0 the speed of sound, and σ_m the modal radiation efficiency. σ_m is approximated using either its pulsating sphere expression or its infinite cylinder expression according to stator dimensions (Timar & Lai 1994). $1/2$ factor in (23) takes into account bakeward and forward-travelling vibration waves.

Sound power level at frequency f is

$$L_w(f) = 10\log_{10}(\sum_m W_m(f)/W_0), \quad W_0 = 10^{-12}W \quad (24)$$

A-weighted total sound power level is finally obtained as

$$L_{wA} = 10\log_{10}\left(\sum_f 10^{0.1(L_w(f)+\Delta L_A(f))}\right) \quad (25)$$

where $\Delta L_A(f)$ shift is a function of human's ear sensitivity.

V. ANALYTICAL EXPRESSION OF MAIN RADIAL FORCE SPECTRUM LINES

This part aims at characterizing the electromagnetic noise spectral content which is the same for noise and vibration. The electromagnetic force spectrum results from the interaction of permeance and mmf spectra, which can be determined using Fourier series. However, airgap flux density is not computed in DIVA on the base of these Fourier series because they are computationally costly.

A. Permeance orders and frequencies

The Fourier series of permeance per unit area is (Brudny 1997, Hesse 1992)

$$\Lambda = \Lambda_0 + \sum_{k_s=1}^{\infty}\Lambda_{k_s}\cos(k_s Z_s \alpha_s) + \sum_{k_r=1}^{\infty}\Lambda_{k_r}\cos\left(k_r Z_r(\alpha_s - \alpha_r)\right) + \frac{1}{2}\sum_{k_s=1}^{\infty}\sum_{k_r=1}^{\infty}\Lambda_{k_s k_r}\{\cos((k_s Z_s - k_r Z_r)\alpha_s + k_r Z_r \alpha_r) + \cos((k_s Z_s + k_r Z_r)\alpha_s - k_r Z_r \alpha_r)\} \quad (26)$$

where

$$\Lambda_0 = \mu_0 A^0 \quad \Lambda_{k_s} = 2\mu_0 A^s f(k_s) \quad \Lambda_{k_r} = 2\mu_0 A^r f(k_r) \quad \Lambda_{k_s k_r} = 4\mu_0 A^{sr} f(k_s) f(k_r)$$

and

$$f(k_s) = \frac{\sin(\pi k_s r_d^s)}{2k_s} \quad f(k_r) = \frac{\sin(\pi k_r r_d^r)}{2k_r}$$

$$A^0 = \frac{1}{g_M}\left(1 + \frac{p_s^f r_d^s}{g^r} + \frac{p_r^f r_d^r}{g^s} + (1+\frac{g_M}{g})\frac{p_s^f r_d^s}{g^r}\frac{p_r^f r_d^r}{g^s}\right)$$

$$A^s = \frac{2p_s^f}{\pi g_M g^r}\left(1 + (1+\frac{g_M}{g})\frac{p_r^f r_d^r}{g^s}\right) \quad A^r = \frac{2p_r^f}{\pi g_M g^s}\left(1 + (1+\frac{g_M}{g})\frac{p_s^f r_d^s}{g^r}\right) \quad A^{sr} = \frac{4p_r^f p_s^f}{\pi^2 g_M g^s g^r}(1+\frac{g_M}{g})$$

$$g_M = g + p_s^f + p_r^f \quad g^s = g + p_s^f \quad g^r = g + p_r^f$$

g is the minimal effective air-gap width whereas g_M is the maximal effective air-gap width. α_r is the angular position of rotor bar number 1 in stator steady frame:

$$\alpha_r(t) = \frac{\omega_1}{p}(1-s)t + \alpha_r^0 \quad (27)$$

p_s^f and p_r^f are the stator and rotor fictitious slot depths, their values are fixed as suggested by (Brudny 1997) proportionally to rotor and stator slot openings ($l_{re}/5$ and $l_{se}/5$). r_d^s and r_d^r are stator and rotor slotting ratios

$$r_d^s = l_{sd}/(l_{sd}+l_{se}) \quad r_d^r = l_{rd}/(l_{rd}+l_{re})$$

Expression (26) allows to easily identify permeance waves orders and frequencies. They are reported in Table II where notation $f_R = f_s(1-s)/p$ is used. When two waves of frequencies and orders (f_1, m_1) and (f_2, m_2) are multiplied, they generate two aditionnal waves (f_1+f_2, m_1+m_2) and (f_1-f_2, m_1-m_2). These new waves can be represented by $(f_1+\eta_{12}f_2, m_1+\eta_{12}m_2)^2$, where the symbol η_{12} can either take the value 1 or -1. Using that symbol instead of ± 1 makes it easier to associate a given frequency to its spatial order.

In Table II, P_0 stands for mean permeance Λ_0, whereas P_s and P_r represent stator and rotor slotting contributions, and P_{sr} their interaction. In this work, low magnitude P_{sr} waves will not be considered for readability purpose. Saturation and eccentricity harmonics will not be discussed neither, but they should be added in this table.

TABLE II

PERMEANCE WAVES FREQUENCIES AND SPATIAL ORDERS

Name/Amplitude	Spatial orders	Frequencies	Comments
P_0	0	0	
P_s	$k_s Z_s$	0	$k_r, k_s \geq 1$
P_r	$k_r Z_r$	$-k_r Z_r f_R$	
P_{sr}	$k_s Z_s + \eta k_r Z_r$	$-\eta k_r Z_r f_R$	

B. Stator mmf orders and frequencies

The same analysis can be carried with mmfs. Stator mmf is the product of stator currents of frequencies f_n^s with stator TFs. Stator TFs do not depend on time, and therefore only bring space harmonics ν_s. Their expression could be obtained from the Fourier expansion of the stator turn function N_0^s illustrated in FIG. 2, as it is going to be done for rotor in section V-C:

$$N_k^s(\alpha_s) = \sum_{n_s=1}^{\infty} \frac{2}{n_s^2 \beta_s(\pi - \beta_s)} \sin(n_r(\alpha_s - \alpha_s^k)) \tag{28}$$

where α_s^k is the k-th slot angular position:

$$\alpha_s^k = \alpha_s^0 + (k-1)\frac{2\pi}{Z_s} \tag{29}$$

However, we are here going to use the work of (Wach 1998) who detailed the space harmonic content of any fractional-slot winding. As the studied machine is double-layer wound, the number of coils per pole and phase m_c equals the number of slots per pole and phase m_s

$$m_s = m_c = \frac{Z_s}{2pq_s} = \frac{27}{12} = \frac{9}{4} = 2 + \frac{1}{4} \doteq I_c + \frac{i}{h} \tag{30}$$

where I_c is the integer part of m_s reduced improper fraction. As $h = 4$ is even, space harmonics ν_s generated by stator TF are given by (Wach 1998)

$$\nu_s = k\frac{2p}{h} = k \qquad k \in \mathbb{N}^* \tag{31}$$

Finally, as the number of phases $q_s = 3$ is prime and odd, the total sum of phase TFs does not contain space harmonics multiple of q_s. Space harmonics brought by the stator mmf in the air-gap are then

$$\nu_s = 1, 2, 4, 5, 7, ... = |p + \epsilon_s q_s h_s| \qquad \epsilon_s = \pm 1, h_s \in \mathbb{N} \tag{32}$$

These theoretical results agree with Fig. 4 simulation. In that figure, the real Fourier transform is used, which does not allow to distinguish the propagation direction of space harmonic fields. For instance, the space harmonic $\nu_s = |p - q_s| = 1$ for $h_s = 1$ rotates backward whereas the stator mmf fundamental space harmonic given by ν_s=p=2 for h_s=0 rotates forward. Integral windings bring space harmonics of the form $|p + \epsilon_s 2pq_s h_s| = p, 5p, 7p, 11p....$

C. Rotor mmf orders and frequencies

Rotor mmf f_{mm}^r is the product of rotor currents with rotor turns functions N_k^r:

$$f_{mm}^r(t, \alpha_s) = \sum_{k=1}^{Z_r} \sum_{m,n} I_{mn}^r \sin\left(s_{mn}\omega_n t - mk\frac{2\pi}{Z_r} + \phi_{mn}^r\right) N_k^r(t, \alpha_s) \tag{33}$$

where $m = \nu_s$ stands for the stator winding space harmonics induced in rotor bars (Henao et al. 2005), I_{mn}^r is the rotor bars peak current computed by the aid of the equivalent circuit described in section II-A, and ϕ_{mn}^r its phase angle. Rotor TF

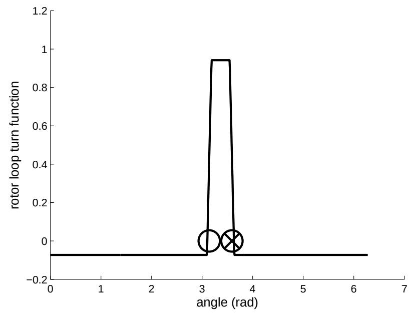

Fig. 7. Single rotor bar turns function (TF) in function of α_s angle, including a linear rise in rotor slot of angular width $2\beta_r$.

spectrum is more complex than stator one because it brings both time and space harmonics. The TF associated to a single bar is plotted in Fig. 7 in stator steady frame.

In a rotor tooth centered frame, this function is even and its Fourier series is

$$N_0^r(\alpha_s) = \frac{\beta_r}{2\pi}(\frac{1}{Z_r} - \frac{1}{2}) + \sum_{n_r=1}^{\infty} A_{n_r} \cos(n_r \alpha_s) \tag{34}$$

where

$$A_{n_r} = \frac{2}{n_r \pi}\left(\frac{2}{\beta_r n_r}\sin(\frac{n_r \pi}{Z_r})\sin(n_r \beta_r) - \sin(n_r(\frac{\pi}{Z_r} + \beta_r))\right)$$

and β_r is the half rotor slot angular opening. The term in $1/n_r^2$ comes from the linear rise in slots, it vanishes when $\beta_r \to 0$. Note that the mean value $\frac{\beta_r}{2\pi}(\frac{1}{Z_r} - \frac{1}{2})$ will disappear when summing on rotor bars in rotor mmf expression (33). The angular position of the k-th bar α_k in the stator steady frame can be written under the form

$$\alpha_r^k(t) = \alpha_r(t) + (k-1)\frac{2\pi}{Z_r} \tag{35}$$

k-th rotor tooth position θ_r^k is then given by

$$\theta_r^k(t) = \frac{1}{2}(\alpha_r^{k+1}(t) + \alpha_r^k(t)) = \alpha_r(t) + (2k-1)\frac{\pi}{Z_r} \tag{36}$$

Finally, the k-th bar turns function is expressed as

$$N_k^r(t, \alpha_s) = N_0^r(\alpha_s - \theta_r^k(t)) \tag{37}$$

In (34), it seems that rotor TF brings all the space harmonics $n_r = 1, 2, 3....$ However, when multiplying by rotor currents and summing on rotor bars mmfs, only space harmonics $n_r = h_r Z_r \pm \nu_s = \nu_r$ have a non-zero contribution. In (33), one can see that the rotor currents of frequency $f_{\nu_s n}^r = s_{\nu_s n}\omega_n$ combine with the rotor TF frequencies $\nu_r f_s(1-s)/p$ and spatial orders ν_r. Resulting spectrum as well as stator's one are summarized in Table III.

TABLE III

ROTOR AND STATOR MMF WAVES FREQUENCIES AND SPATIAL ORDERS

Name/Amplitude	Spatial orders	Frequencies	Comments
F_s	$\nu_s = p + \epsilon_s q_s h_s$	$\epsilon_s f_n^s$	$h_s \geq 0$
F_r	$\nu_r = h_r Z_r + \epsilon_r \nu_s$	$\nu_r f_R + \epsilon_r f_{\nu_s n}^r$	$h_r \geq 0$

D. Flux density orders and frequencies

Air-gap flux density is the product of permeance waves of type P_0, P_s and P_r with mmf waves of type F_s and F_r, its spectrum is given by their 6 possible combinations (Table IV).

[2]Using that notation, the waves (m, f) and $(-m, -f)$ are the same.

TABLE IV

FLUX DENSITY WAVES FREQUENCIES AND SPATIAL ORDERS

Name/Amplitude	Spatial orders	Frequencies
P_0F_s	$\eta_{0s}\nu_s$	$\eta_{0s}\epsilon_s f_n^s$
P_0F_r	$\eta_{0r}\nu_r$	$\eta_{0r}(\nu_r f_R + \epsilon_r f_{\nu_s n}^r)$
P_sF_s	$k_sZ_s + \eta_{ss}\nu_s$	$\eta_{ss}\epsilon_s f_n^s$
P_sF_r	$k_sZ_s + \eta_{sr}\nu_r$	$\eta_{sr}(\nu_r f_R + \epsilon_r f_{\nu_s n}^r)$
P_rF_s	$k_rZ_r + \eta_{rs}\nu_s$	$-k_rZ_r f_R + \eta_{rs}\epsilon_s f_n^s$
P_rF_r	$k_rZ_r + \eta_{rr}\nu_r$	$-k_rZ_r f_R + \eta_{rr}(\nu_r f_R + \epsilon_r f_{\nu_s n}^r)$

E. Radial force orders and frequencies

Finally, to obtain the electromagnetic force spectrum, one has to multiply all the flux density waves of Table IV one with another. Resulting lines are presented in Table V where high spatial order lines (e.g. the interaction of wave P_sF_s with itself which leads to a $2k_sZ_s \pm 2\nu_s$ order [3]) and redundant lines like the interactions $P_sF_sP_rF_r$ and $P_sF_rP_rF_s$ have been removed. As these main lines are expressed in function of stator and rotor space harmonics ν_s and ν_r, their expressions are general and can be applied to any stator and rotor winding.

TABLE V

MAIN RADIAL FORCE LINES FREQUENCIES AND SPATIAL ORDERS. FOR INSTANCE, $\epsilon_r = -\epsilon_s = 1$, $\nu_s = \nu_r = p$, $k_r = k_s = 1$ AND $\eta_{rr} = -\eta_{ss} = 1$ GIVE A FORCE LINE L_3 OF ORDER $Z_s - Z_r - 2p = 2$ AND FREQUENCY $(Z_r - p)f_R + f_s - sf_s = Z_r f_s(1-s)/p$.

Name/Amplitude	Spatial orders	Frequencies	
$L_1 = P_sF_sP_sF_r$	$\eta_{ss}\nu_s - \eta_{sr}\nu_r$	$\eta_{ss}\epsilon_s f_{n_1}^s - \eta_{sr}(\nu_r f_R + \epsilon_r f_{\nu_s n_2}^r)$	
$L_2 = P_sF_sP_rF_s$	$k_sZ_s - k_rZ_r + \nu_s\eta_{ss} - \nu_s'\eta_{rs}$	$k_rZ_r f_R + f_{n_1}^s\epsilon_s\eta_{ss} - f_{n_2}^s\epsilon_s'\eta_{rs}$	
$L_3 = P_sF_sP_rF_r$	$k_sZ_s - k_rZ_r + \eta_{ss}\nu_s - \eta_{rr}\nu_r$	$(k_rZ_r - \eta_{rr}\nu_r)f_R + \epsilon_s\eta_{ss}f_{n_1}^s - \epsilon_r\eta_{rr}f_{\nu_s n_2}^r$	
$L_4 = P_sF_rP_rF_r$	$k_sZ_s - k_rZ_r + \eta_{sr}\nu_r' - \eta_{rr}\nu_r$	$f_R(k_rZ_r + \eta_{sr}\nu_r' - \eta_{rr}\nu_r) + \epsilon_r\eta_{sr}f_{\nu_s n_1}^r - \epsilon_r'\eta_{rr}f_{\nu_s n_2}^r$	*
$L_5 = P_rF_sP_rF_r$	$\eta_{rs}\nu_s - \eta_{rr}\nu_r$	$\eta_{rs}\epsilon_s f_{n_1}^s - \eta_{rr}(\nu_r f_R + \epsilon_r f_{\nu_s n_2}^r)$	
$L_6 = P_0F_sP_0F_s$	$\eta_{0s}\nu_s - \eta_{0s}'\nu_s'$	$\epsilon_s\eta_{0s}f_{n_1}^s - \epsilon_s'\eta_{0s}'f_{n_2}^s$	
$L_7 = P_0F_rP_0F_r$	$\eta_{0r}\nu_r - \eta_{0r}'\nu_r'$	$f_R(\eta_{0r}\nu_r - \eta_{0r}'\nu_r') + \epsilon_r\eta_{0r}f_{\nu_s n_1}^r - \epsilon_r'\eta_{0r}'f_{\nu_s n_2}^r$	
$L_8 = P_0F_rP_0F_s$	$\eta_{0r}\nu_r - \eta_{0s}\nu_s$	$\eta_{0r}(\nu_r f_R + \epsilon_r f_{\nu_s n_1}^r) - \epsilon_s\eta_{0s}f_{n_2}^s$	

In sinusoidal case, $f_n^s = f_s$, and as a consequence lines L_1, L_5, L_6, L_7 and L_8 have low frequencies (typically $2f_s \leq 200$ Hz) and might be covered by mechanical noise. Other lines associated to fundamental mmfs ($\nu_s = \nu_r = p$, $\epsilon_s = -1$, $\epsilon_r = 1$ and $f_{\nu_s 1}^r = sf_s$) have all the following form:

$$F_{2,3,4} = f_s((1-s)\frac{k_rZ_r}{p} \pm |_0^2) \tag{38}$$

They are associated to spatial orders of the form

$$M_{2,3,4} = \pm k_sZ_s \mp k_rZ_r \pm |_0^{2p} \tag{39}$$

Among these lines, the most important ones are L_2 because they do not involve rotor mmf waves of amplitude $F_r \ll F_s$. These lines are mostly responsible for electromagnetic noise in sinusoidal case, because they can be associated to low spatial orders (Jordan 1950). Notice that such lines, as they are caused by fundamental current, generally remain in case of a non-sinusoidal supply.

In non-sinusoidal case, the force lines L_1, L_5, L_6, L_7 and L_8 can be located at high frequencies and therefore significantly contribute to acoustic noise. We can see that they are necessarily associated to orders

$$M_{1,5,6,7,8} = 0 \quad \text{or} \quad 2p \tag{40}$$

when considering mmf space fundamentals. Among them, lines of highest amplitude are of the form L_6 and occur at frequencies $F_6 = |\pm f_s \pm f_n^s|$ (Lo, Chan, Zhu, Xu, Howe & Chau 2000). Lines L_7 may be neglictible as they involve the square amplitude of rotor mmf waves, and occur at low frequencies. Other important lines in PWM case are therefore L_1 and L_5, which have exactly the same form of orders and frequencies, and L_8. Among them, the main lines are obtained taking the fundamental time harmonic of rotor current, and the corresponding frequencies are found to be also of the form

$$F_{1,5,6,8} = |\pm f_s \pm f_n^s| \tag{41}$$

[3]A high ν_s and a low k_s, e.g. $k_s = 1$, could result in a low spatial order. However, the higher ν_s is, the lower the amplitude of stator mmf wave F_s is.

VI. Simulation Results

A first simulation was run at nominal frequency $f_s = 50$ Hz, without considering stator space harmonics induced in rotor currents. Computed A-weighted noise spectrum on the whole audible range [0 Hz, 20 kHz] is displayed in Fig. 8. Note that such a precise and wide spectrum could not be obtained with finite element (for vibrations) and boundary element methods (for sound pressure): these numerical methods can hardly compute a noise spectrum up to 3200 Hz, and with a prohibitive computational time of several hours, whereas the analytical model of DIVA runs in a few seconds on a 2GHz laptop.

Simulated sound power level reaches 58 dBA: as it was observed during tests, the machine is not very noisy at this particular speed and under sinusoidal supply, because no magnetic line really emerges from the spectrum.

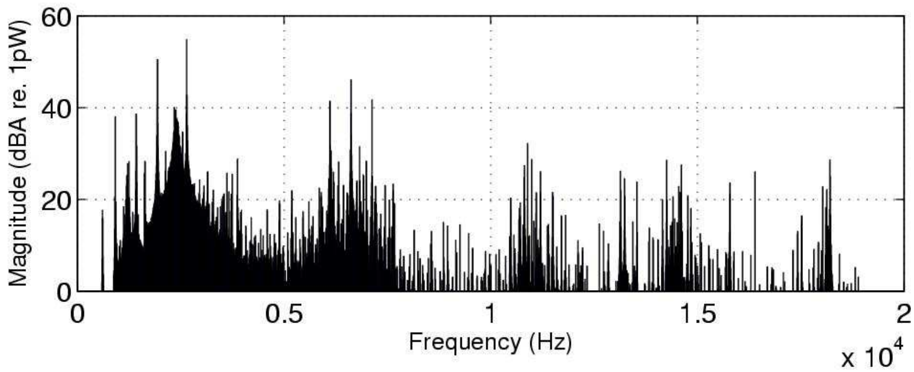

Fig. 8. Simulated A-weighted audible electromagnetic noise L_{wA} (dBA) in on-load sinusoidal case (f_s= 50 Hz, s = 3.05 %)

In order to properly interpretate these lines, it can be useful to find their associated spatial order. It can be done using the analytical results of previous section, but numerically it is also possible to compute each spectrum line without taking into account the acoustic power radiated by a particular spatial mode, and then quantify the contribution of each spatial mode to each spectrum line. This contribution is plotted in Fig. 9 in the range [500 Hz, 3000 Hz] where the highest vibration lines appear.

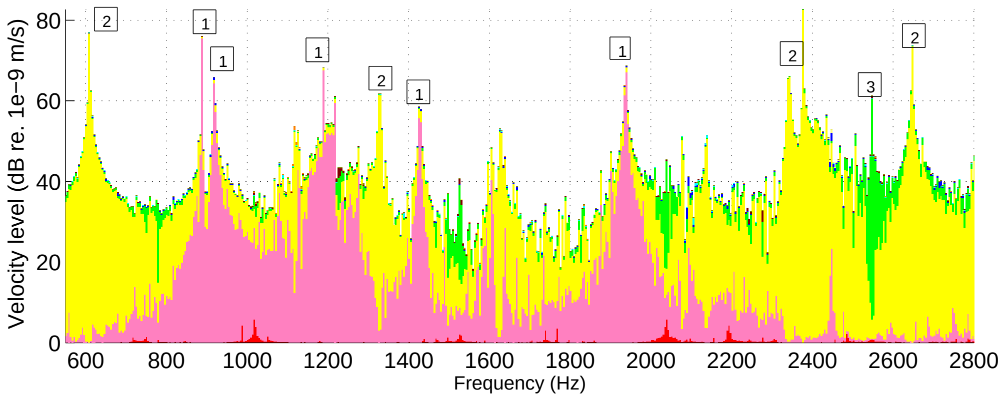

Fig. 9. Simulated vibration velocity spectrum with spatial mode contribution of each line (f_s= 50 Hz, s = 3.05 %). The numbers indicate the spatial orders of vibration lines.

We can see that the main lines have mode numbers m=1,2 and 3. For instance, a line of order 1 occurs at 1935 Hz. Order number 1 can be obtained with $1 = 3Z_s - 4Z_r + 2p$ i.e. $k_r = 4$. We can see that the 1935 Hz frequency precisely corresponds to the form $F_2 = f_s(4(1-s)\frac{Z_r}{p} - 2)$ for η_{ss}=1 and η_{rs}=-1. In the same way, a line of order $2 = Z_s - Z_r - 2p$ occurs at 610 Hz which corresponds to $F_2 = f_s((1-s)\frac{Z_r}{p} + 2)$ Hz (k_r=4, η_{ss}=-1 and η_{rs}=1). Finally, a line of order $3 = 4Z_s - 5Z_r$ occurs at 2550 Hz of the form $F_2 = f_s(5(1-s)\frac{Z_r}{p})$ (k_r=5, η_{ss}=η_{rs}=1). These few examples show how the simulations results correctly fit to previous analytical results.

Modal contribution analysis can be also carried with sound power level L_w at variable speed (Fig. 10), that is to say during a motor speed ramp at constant flux. Sound power level is computed by simulating nearly one rotor turn, so if the speed do not significantly change during this turn (which is a reasonable assumption in our case), the variable-speed level can be obtained by computing sound power levels at each speed step.

Such a graph allows for instance to see that around supply frequency $f_s = 30$ Hz, it is mode $m = 1$ which radiate the most, whereas at $f_s = 45$ Hz it is $m = 2$. The 30 Hz resonance comes from the match between the magnetic line $f_s(4(1-s)Z_r/p-2)$ which has been previously pointed out and the 1200 Hz mode number 1 natural frequency.

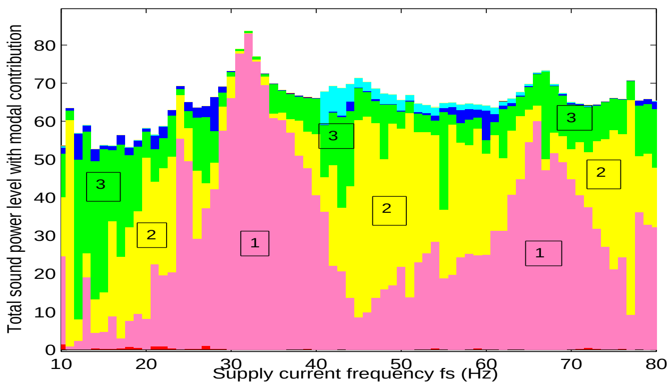

Fig. 10. Variable-speed simulation with spatial orders contribution to total sound power level L_w (dB). The numbers indicate the spatial orders.

Previous simulations show that some odd spatial modes (m=1,3) play an important role in noise radiation. Integral windings impose an even slot numbers: consequently, $\overline{Z_s} = \overline{0}$ ($\overline{n}$ stands for the congruence modulo 2 operator, i.e. $\overline{n} = \overline{0}$ if n is even and $\overline{n} = \overline{1}$ otherwise). In that case, as $\nu_s = p(2q_s h_s + \epsilon_s)$, we have $\overline{\nu}_s = \pm\overline{p}$. Moreover, for a squirrel cage rotor, $\overline{\nu}_r = \overline{h}_r\overline{Z}_r \pm \overline{\nu}_s = \overline{0}$ (assuming that the number of bars is even, which is common in order to avoid high torque pulsations). Under these conditions, one can easily check in Tab. V that all magnetic force lines have necessary even spatial orders. For instance,

$$\overline{M} = \pm\overline{k}_s\overline{Z}_s \mp \overline{k}_r\overline{Z}_r \pm |_{\overline{0}}^{\overline{\nu}_s\pm\overline{\nu}_r} = \overline{0} \qquad (42)$$

When using an odd number of stator slots, which necessarily impose a fractional-slot winding as $Z_s/(2pq_s)$ cannot be integral, we do not necessarily have $\overline{M} = \overline{0}$: the electromagnetic power brought by Maxwell air-gap pressure can dissipate as vibrations through all the stator deflection modes. Therefore, acoustic power is more uniformly distributed in spatial modes and if a resonance occur, it will be smaller than in traditonal even slot number combination machines. However, it also means that electromagnetic pressure can excite some odd modes natural frequency.

VII. Conclusion

An analytical noise-predictive model of the induction machine and its converter was presented. The expression of main noise spectrum lines frequencies and spatial orders, including stator winding and rotor bars space harmonics, as well as PWM time harmonics, was derived analytically. These theoretical results were favorably compared to simulations and expriments in on-load sinusoidal case.

Saturation and eccentricity effects have not been discussed in that article, although they are taken into account in DIVA. Saturation modifies the air-gap flux density shape, which adds new harmonics in Maxwell forces spectrum. This new harmonic content can be modelled by adding saturation permeance waves (Maliti 2000). Dynamic and static eccentricities also change permeance waves, and can be easily taken into account (Toliyat & Arefeen 1996) without increasing computational cost.

Future work will address the effect of PWM on magnetic noise generation, and detail other experimental validations of the developed simulation tool.

References

Ait-Hammouda, A. (2005), Prédimensionnement et étude de sensibilité vibro-acoustique de machines courant alternatif et vitesse variable, PhD thesis, Université des Sciences et des Technologies de Lille, France.

Besnerais, J. L., Fasquelle, A., Hecquet, M., Lanfranchi, V. & Brochet, P. (2006), A fast noise-predictive multiphysical model of the PWM-controlled induction machine, *in* 'Proc. of the International Conference on Electrical Machines (ICEM'06)', Chania, Greece.

Bossio, G., Angelo, C. D., Solsona, J., Garcia, G. & Valla, M. (2004), 'A 2-D model of the induction machine: an extension of the modified winding function approach', *IEEE Trans. on Energy Conversion* **19**(1).

Brudny, J. (1997), 'Modélisation de la denture des machines asynchrones : phénomènes de résonances', *Journal of Physics III* **37**(7).

Cremer, L., Heckl, M. & Ungar, E. (1988), *Structure-Borne Sound*, Springer-Verlag.

Gieras, J. (2005), *Noise of polyphase electric motors*, CRC Press.

Henao, H., Razik, H. & Capolino, G. (2005), 'Analytical approach of the stator current frequency harmonics computation for detection of induction machine rotor faults', *IEEE Trans. on Ind. App.* **41**(3).

Hesse, H. (1992), ‘Air gap permeance in doubly-slotted asynchronous machines’, *IEEE Trans. on Energy Conversion* **7**(3).

Hubert, A. (2000), Contribution l’étude des bruits acoustiques générés lors de l’association machines électriques - convertisseurs statiques de puissances - application la machine asynchrone, PhD thesis, Université des Technologies de Compiègne, France.

Hubert, A. & Friedrich, G. (2002), ‘Influence of power converter on induction motor acoustic noise: interaction between control strategy and mechanical structure’, *Electric Power Applications, IEE Proceedings* **149**.

Joksimovic, G., Djurovic, M. & Penman, J. (2001), ‘Cage rotor MMF : winding function approach’, *IEEE Power Engineering Review* **21**(4).

Jordan, H. (1950), *Electric motor silencer - formation and elimination of the noises in the electric motors*, W. Giradet-Essen editor.

Lo, W., Chan, C., Zhu, Z., Xu, L., Howe, D. & Chau, K. (2000), ‘Acoustic noise radiated by PWM-controlled induction machine drives’, *IEEE Trans. on Industrial Electronics* **47**(4).

Maliti, K. (2000), Modelling and analysis of magnetic noise in squirrel-cage induction motors, PhD thesis, Stockholm.

Matsuse, K., Hayashida, T., Kubota, H. & Yoshida, T. (1994), ‘Analysis of inverter-fed high speed induction motor considering crosspath resistance between adjacent rotor bars’, *IEEE Trans. Ind. Appl.* **30**(3).

Salminen, P. (2004), Fractional slot permanent magnet synchronous motors for low speed application, PhD thesis, Lappeenranta University of Technology, Finland.

Timar, P. & Lai, J. (1994), ‘Acoustic noise of electromagnetic origin in an ideal frequency-converter-driven induction motor’, *IEE Proceedings on Electrical Power Applications* **141**(6).

Toliyat, A. & Arefeen, M. (1996), ‘A method for dynamic simulation of air-gap eccentricity in induction machines’, *IEEE Trans. on Industry Applications* **32**(4).

Verma, S. & Balan, A. (1998), ‘Experimental investigations on the stators of electrical machines in relation to vibration and noise problems’, *IEE Proceedings on Electrical Power Applications* **145**(5).

Wach, P. (1998), ‘Algorithmic method of design and analysis of fractional-slot windings of AC windings’, *Electrical Engineering* **81**(3).

Yang, S. J. (1981), *Low noise electrical motors*, Clarendon Press, Oxford.